Marine Geology 419 (2020) 106076

Contents lists available at ScienceDirect

Marine Geology

journal homepage: www.elsevier.com/locate/margo

Modern sedimentary processes at the heads of Martínez Channel and Steffen Fjord, Chilean Patagonia

Elke Vandekerkhove[a,*], Sebastien Bertrand[a], Eleonora Crescenzi Lanna[a], Brian Reid[b], Silvio Pantoja[c]

[a] Renard Centre of Marine Geology, Department of Geology, Ghent University, Krijgslaan 281 S8, 9000 Gent, Belgium
[b] Centro de Investigación en Ecosistemas de la Patagonia (CIEP), Universidad Austral de Chile, Francisco Bilbao 323, Coyhaique, Chile
[c] Departamento de Oceanografía and Centro de Investigación Oceanográfica COPAS Sur-Austral, Universidad de Concepción, Concepción, Chile

ARTICLE INFO

Editor: Michele Rebesco

Keywords:
Chilean fjords
Multibeam bathymetry
Submarine channel
Turbidity current
Sediment transport

ABSTRACT

Chilean fjord sediments constitute high-resolution archives of climate and environmental change in the southern Andes. To interpret such records accurately, it is crucial to understand how sediment is transported and deposited within these basins. This issue is of particular importance in glaciofluvial Martínez Channel and Steffen Fjord (48°S), due to the increasing occurrence of Glacial Lake Outburst Floods (GLOFs) originating from outlet glaciers of the Northern Patagonian Icefield. Hence, the bathymetry of the head of Martínez Channel and Steffen Fjord was mapped at high resolution and the grain-size and organic carbon content of grab sediment samples were examined. Results show that the subaquatic deltas of Baker and Huemules rivers at the head of Martínez Channel and Steffen Fjord, respectively, are deeply incised (up to 36 m) by sinuous channels. The presence of sediment waves and coarser sediments within these channels imply recent activity and sediment transport by turbidity currents. Although several triggering mechanisms are possible, we argue that elevated river discharge and the associated relatively high suspended sediment loads is the main cause of the occurrence of turbidity currents at the head of these fjords and are of key importance in shaping the fjord's subaquatic morphology. This study shows that the heads of Martínez Channel and Steffen Fjord are dynamic sedimentary environments with rapidly migrating channels. It highlights the importance of site selection and multi-coring in any future project aimed at reconstructing environmental change using the sediments of either fjord.

1. Introduction

Fjords are sensitive environments at the interface between the ocean and the adjacent mountainous land masses. They occur in mid to high latitude regions and their sediment infill is, or was, closely related to glacier activity (e.g., Syvitski et al., 1987). Consequently, fjords can hold important sediment records of these changing glacial conditions during the Holocene. Patagonian fjord sediments, in particular, are increasingly recognized as high-resolution archives of climate and environmental changes. Previous studies have used these sediment archives to reconstruct past changes in glacier variability (Bertrand et al., 2012, 2017), sea surface temperature (Sepúlveda et al., 2009; Caniupán et al., 2014), precipitation (Lamy et al., 2010; Bertrand et al., 2014), and seismic activity (Piret et al., 2017a; Wils et al., 2018).

A fjord area that is increasingly attracting the attention of scientists working in Patagonia is the Baker-Martínez fjord system (48°S), particularly due to the increasing occurrence of Glacial Lake Outburst Floods (GLOFs) originating from the rapidly retreating outlet glaciers of the Northern Patagonian Icefield (NPI; Harrison et al., 2007; Lopez et al., 2010; Dussaillant et al., 2010; Davies and Glasser, 2012; Wilson et al., 2018). Although the impact of modern GLOFs on the hydrography and ecology of the Baker-Martínez fjord system has recently received a fair amount of attention (e.g., Marin et al., 2013; Meerhoff et al., 2018), the sedimentary processes taking place in the fjords during GLOFs remain mostly unknown. This is largely due to the lack of a detailed bathymetric map, for which only few manual depth soundings have been acquired by the Chilean Navy Hydrographic and Oceanographic Service (Servicio Hidrográfico y Oceanográfico de la Armada, 2001). Accurate bathymetric information is also an essential prerequisite to any detailed study of the fjord's sediments to reconstruct the regional GLOF history, which is of both scientific and societal interest. Finally, an improved bathymetric map is increasingly important for the future development of the region (e.g., subsea infrastructure, town expansion).

General fjord sedimentation models indicate that the sediment

* Corresponding author.
E-mail address: Elke.Vandekerkhove@UGent.be (E. Vandekerkhove).

https://doi.org/10.1016/j.margeo.2019.106076
Received 26 April 2019; Received in revised form 29 October 2019; Accepted 31 October 2019
Available online 05 November 2019
0025-3227/

entering a fjord is separated into two components: (1) a coarser bedload, which gets deposited quickly onto the delta, and (2) a buoyant hypopycnal plume, which flows on top of a salty, warmer, water mass, creating a two-layer flow typical for fjord systems (Syvitski and Shaw, 1995). As rivers in Chilean Patagonia discharge large amounts of sediment-laden freshwater into the fjords, the two-layer circulation varies seasonally according to river discharge, which increases in summer due to glacier and snowmelt (Iriarte et al., 2014). As the buoyant plume flows towards the ocean, suspended sediment settles in response to the decreasing velocity, increasing salinity, and due to flocculation, agglomeration, and pelletization of finer particles (Syvitski, 1991). Previous bathymetric surveys have shown the diverse morphologies existing in Patagonian fjords and how different glaciofluvial sedimentary processes are important in shaping the fjord bottoms (e.g., DaSilva et al., 1997; Boyd et al., 2008; Rodrigo, 2008; Araya Vergara, 2011; Dowdeswell and Vásquez, 2013).

To better understand the sedimentary processes taking place at the heads of Martínez Channel and Steffen Fjord (48°S), this paper presents approximately 100 km^2 of new high-resolution multibeam bathymetry acquired in 2016. The distinctive morphological features are then thoroughly described and discussed. In addition, grab sediment samples are examined for their physical properties and organic carbon content to understand recent fjord sedimentary processes related to the discharge of water and sediment by the main rivers entering the fjords.

2. Setting

Martínez Channel and Steffen Fjord are located in Chilean Patagonia (47.8°S–73.6°W; Fig. 1a), between the Northern Patagonian Icefield (NPI) and the Southern Patagonian Icefield (SPI). This mountainous region is characterized by a complex island and channel landscape that was formed by extensive glacial erosion. During the Quaternary, the NPI and SPI have contracted and expanded several times (Kaplan et al., 2004; Douglass et al., 2005; Harrison and Glasser, 2011), converging during glacial periods into the larger Patagonian Ice Sheet (PIS: 38–56°S; Caldenius, 1932). After the Last Glacial Maximum (LGM), PIS glaciers started to shrink and new drainage routes opened (Harrison and Glasser, 2011; García et al., 2012; Glasser et al., 2012; Glasser et al., 2016), eventually leading to the formation of many fjords and lakes. Discharge of large quantities of ice and meltwater was reorganized westwards towards the Pacific Ocean from 10 kyr onwards (Glasser et al., 2016), or earlier (13.5 kyr ago; Hubbard et al., 2005).

The glacierized region of Chilean Patagonia is increasingly prone to GLOFs due to the rapid retreat of most NPI outlet glaciers (Harrison et al., 2007; Lopez et al., 2010; Davies and Glasser, 2012; Wilson et al., 2018). Most recent GLOFs in the region originate from the Colonia river valley (Dussaillant et al., 2010; Fig. 1a), where previous studies have shown the presence of flood events in 1896–1897, 1914–1917, 1944, and 1963 (Lliboutry, 1965; Tanaka, 1980; Winchester and Harrison, 2000). Since April 2008, the Colonia river valley experiences repeated GLOFs related to the abrupt emptying of Cachet 2 Lake (Dussaillant et al., 2010; Jacquet et al., 2017). During such GLOF events, Baker River triples in discharge (Dussaillant et al., 2010) and river suspended sediment concentrations increase 8-fold due to erosion of lake-bed and valley-fill deposits in the watershed (Bastianon et al., 2012). Similar flood events are also occurring in the Huemules river valley, where 10 GLOFs were documented between 1985 and 2013 (Aniya, 2014).

The Baker-Martínez fjord system connects the terrestrial environments of Patagonia with the Pacific Ocean (Fig. 1a). Its main tributary is Baker River, which drains most of the eastern side of the NPI and constitutes the largest river in Chile in terms of volume of water. The river originates from Bertrand Lake, which is fed by General Carrera Lake, and flows southwards. Baker River discharge ranges from 600 (winter) to 1200 (summer) m^3/s, and it reaches up to 4200 m^3/s during GLOFs (Dirección General de Aguas, DGA, Chile; Jacquet et al., 2017). According to Quiroga et al. (2012), some of the GLOFs carry an estimated 1.0 to 1.5 × 10^5 tons of sediment to the fjord and may contribute up to 5% of the annual fine sediment load. Baker River discharges at the head of Martínez Channel near the town of Caleta Tortel, where it splits into one main and two smaller outlet channels (Fig. 1b). On the fan-shaped aerial delta, which covers approximately 14 km^2, several smaller abandoned channels are visible.

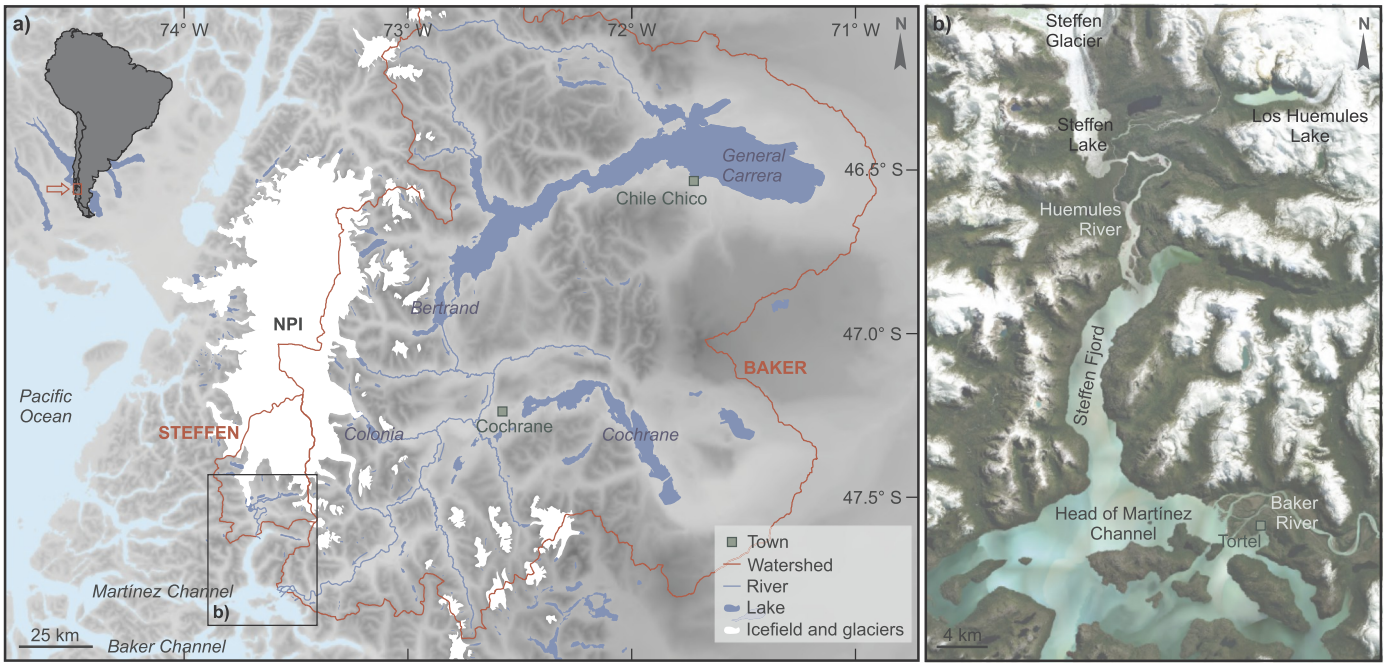

Fig. 1. Location of Steffen Fjord and Martínez Channel in Chilean Patagonia. (a) Watersheds of Huemules and Baker rivers (in red), which are the main tributaries of Steffen Fjord and Martínez Channel, respectively. The limits of the watersheds under the Northern Patagonian Icefield (NPI) are from Lopez et al. (2010). (b) Location of Baker and Huemules rivers at the heads of Martínez Channel and Steffen Fjord, respectively (Global Mapper World Imagery). The white patches correspond to snow and ice. (For interpretation of the references to color in this figure legend, the reader is referred to the web version of this article.)

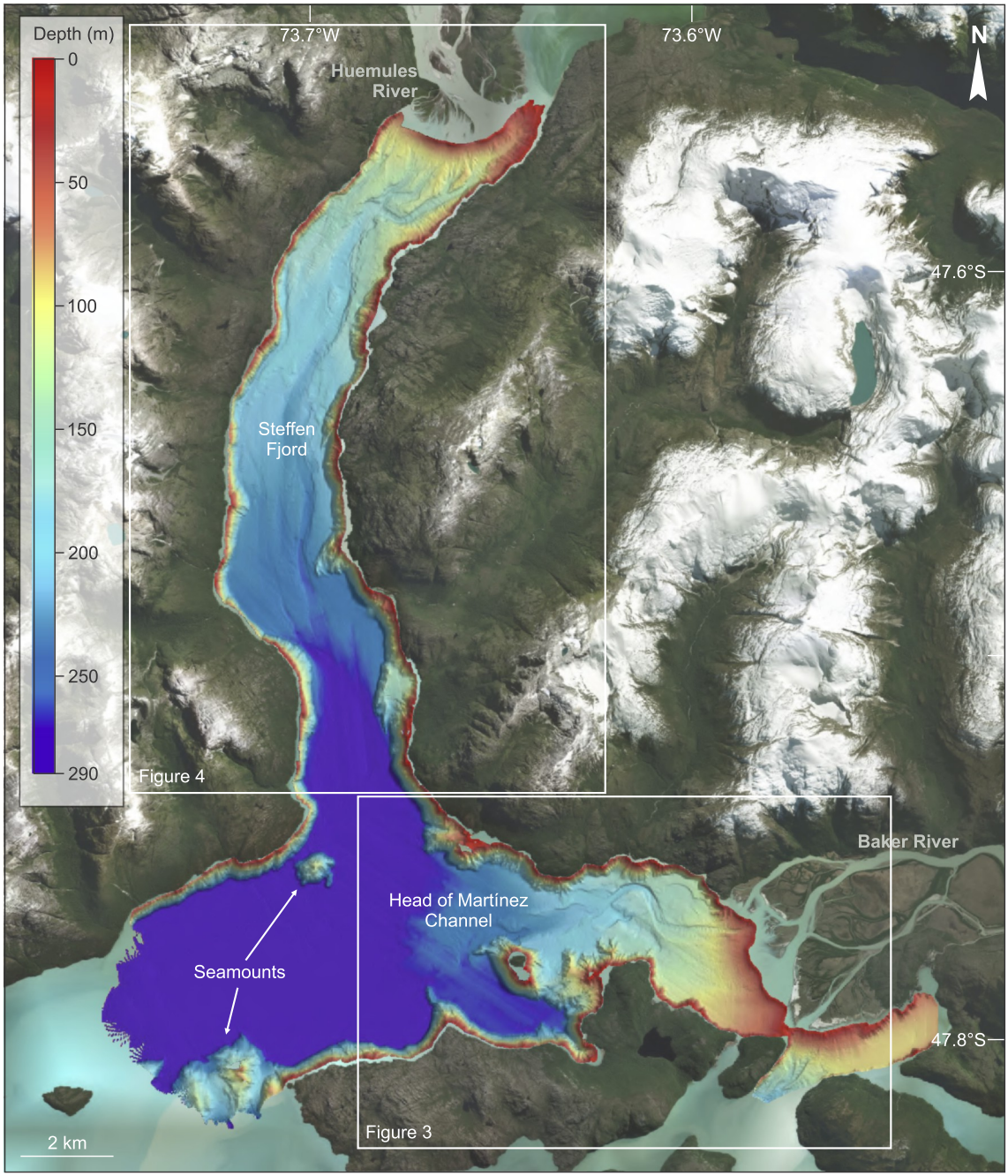

Fig. 2. Bathymetry of Steffen Fjord and of the head of Martínez Channel.

Steffen Fjord is situated immediately to the south of the NPI and it is mainly fed by meltwater from Steffen Glacier via Huemules River. It is an elongated north-south orientated basin, with a total length of approximately 20 km and an average width of 2.5 km (Fig. 1b). Steffen Glacier is the third largest glacier of the NPI with a surface area of 428.3 km^2 (Lopez et al., 2010), which drains most of the southern part of the icefield (Fig. 1a). Over the past decades, the frontal retreat of Steffen Glacier has accelerated from 0.5 km^2/yr (1979–2001) to 1.2 km^2/yr (2001 − 2011), resulting in an ice surface loss of 12 km^2 between 2001 and 2011 (López and Casassa, 2011). Similar to Baker River, Huemules River has a glacial regime due to the large input of meltwater from Steffen Glacier. At the mouth of Huemules River, water flows into Steffen Fjord through one main channel, forming a ~3.6 km^2 fan-shaped delta that encompasses the entire width of the fjord. To the south, surface waters from Steffen Fjord join Martínez Channel and continue flowing westwards towards the Pacific Ocean. Although GLOFs have been documented along Huemules River (Aniya, 2014; DGA, 2019), the river is not equipped with a permanent discharge monitoring station. The exact hydrological conditions during GLOFs are therefore not known.

3. Material and methods

3.1. Multibeam bathymetry

The bathymetry of the head of Martínez Channel and of Steffen Fjord was mapped with an ELAC Seabeam 1050 system in austral winter 2016 to avoid the influence of large sound velocity variations due to variable freshwater input. A mounting frame holding the two 50 kHz transducers at a 120° angle, was installed at the bow of the *R/V*

Sur-Austral (COPAS Sur-Austral, Chile). In order to correct for roll, pitch, and heave movements, an Octans Motion Sensor (IXSEA) was placed on the mounting pole above the transducers. CTD measurements were continuously recorded at the water surface (approximately 1 m depth) using a Valeport Modus CTD. To correct for sound velocity changes with depth, a total of 24 vertical CTD profiles were taken with an RBR Maestro, operating at a sampling rate of 6 Hz and vertical speed of 1 m/s. These CTD profiles were collected on a daily basis and were evenly distributed over the mapped area (Supplementary Fig. A). The multibeam data were processed with *Caris HIPS and SIPS v9.1*, including tide correction based on tide tables at Caleta Tortel (maximum tidal range of 1.9 m). The final bathymetric maps have a grid resolution of 5 m and were created using *Fledermaus v7*.

3.2. Grab sediment samples

A total of 45 surface sediment samples were collected in February 2017 aboard the *R/V Sur-Austral,* using a Van Veen grab sampler (0.008 m^3) attached to a pneumatic winch. A small shovel was used to collect subsamples. All samples were freeze dried. Grain-size measurements of the lithogenic fraction were conducted with a Malvern Mastersizer 3000 particle size analyzer (Ghent University, Belgium). In order to remove organic matter, all samples were pre-treated with 2 ml of a 30% hydrogen peroxide (H_2O_2) solution added to 10 ml of demineralized water containing the suspended sample. Additionally, 1 ml of 10% hydrochloric acid (HCl) and 1 ml of 2 N sodium hydroxide (NaOH) were added to remove carbonate and biogenic silica, respectively. After rinsing the sample, flocculation was avoided by shortly boiling the samples with sodium hexametaphosphate (calgon). Measuring times of 12 s with 10% sonification were used. Total Organic Carbon (TOC) content was determined by analyzing the samples with an elemental analyzer at the Stable Isotope Facility (UC Davis, California, USA). To remove possible inorganic carbon, all samples were treated with 1 N sulfurous acid prior to analysis (Verardo et al., 1990).

4. Results

4.1. Basin morphology

The swath bathymetry imagery indicates that the basin floor (where Steffen Fjord and Martínez Channel merge) is relatively flat, varying on average from 280 to 285 m depth, with a maximum measured water depth of 290 m (Fig. 2). Steep-walled fjord slopes (up to 75°) occur close to the shorelines. Two seamounts are also visible on the flat basin floor. Closer to the river mouths, the bathymetry shows well-developed deltas with several subaquatic morphological features. These features are presented separately for the head of Martínez Channel and Steffen Fjord below.

4.1.1. Head of Martínez Channel

The morphology in front of Baker river mouth is characterized by a large subaquatic delta, with depths that gradually increase from 0 to 266 m (Fig. 3). The proximity of islands in front of the delta obstructs the development of a complete subaquatic delta. The delta slope has a concave profile with a slightly higher slope gradient in the shallower part of the delta (3.4° up to 2 km from the Baker river mouth) compared to the mid-slope region (2°; Figs. 3 and 4). The maximum extent of the submarine delta is located approximately 7.9 km west of the delta margin where a distributary fan can be observed (Fig. 3b). The submarine delta is incised by two prominent channels that are bounded by elevated sediment ridges or levees in the upper slope as well as in the mid-slope delta region (Fig. 3b). The meandering channel west of the main river mouth cuts up to 26 m deep in the sediment and has a total length of approximately 8 km. It has an average width of 140 m and measures 400 m at its widest point (Fig. 4a–c). The channel deviates counterclockwise along-slope Vigía Island and it terminates at a 266 m-deep flat fjord bottom where a lobe-shaped depositional fan is formed (Fig. 3). The second channel is smaller and located in front of the southern branch of Baker River, confined between Morgan and Barrios Islands, where several smaller submarine chutes and channels converge into one single channel. The latter has an average incision depth of 6 m and an average width of 160 m. Bathymetric data for this channel is incomplete so its southern limit is unknown.

Within the axial channels at the head of Martínez Channel, crescent-shaped transverse bedforms are present (Fig. 3b–c). These bedforms occur at regular intervals from a depth of 60 to 172 m. The wavelength of the ridges increases with distance from the delta margin, from 22.5 m at a depth of 60 m to 115 m at a depth of 172 m. The slope of their lee side is on average 13° but can go up to 21° (Fig. 4d). Similar bedforms, although more irregularly shaped, appear in the unchannelized region on the upper slope of the delta, parallel to the delta margin (Fig. 3b, d). These creep-like features of scours and ridges continue downslope approximately 1.7 km from the Baker delta lip to a depth of 138 m (Figs. 3b and 4a). They cover an area of 3.6 km^2 and occur where the slope gradient is between 5 and 15°. The ridges are 1.5 to 5.5 m high and measure up to 700 m in width. In addition, distinctive erosive features, i.e., gullies and remnant channel walls, are visible on the subaquatic part of the delta (Fig. 3b). At the margin of the San Martin river inlet, situated west of Baker River, a smaller fluvial-fed depocenter can be observed (Fig. 3b). It is incised by several gullies and terminates at the western channel. Finally, a head scarp just north of Vigía Island, with a slope angle of 80°, suggests the occurrence of a submarine slope failure (Fig. 3).

4.1.2. Steffen Fjord

The shallow part of the Huemules subaquatic delta is characterized by several gullies that converge into one well-developed channel (Figs. 5 and 6). This channel extends up to 11.5 km to the south in Steffen Fjord and it opens into a flat basin at a depth of 265 m. It has an average width of 185 m and measures 550 m at it widest point. The maximum incision depth is 36 m and channel levees can be observed in the mid-slope region (Fig. 6b). At approximately 3.6 km from the Huemules river mouth, the channel deviates slightly around a subaquatic feature. As at the head of Martínez Channel, crescent-shaped ridges or transverse bedforms are visible within the gullies and channel, although to a lesser extent (Figs. 5 and 6c). These ridges are observed up to 2 km from the Huemules delta lip down to a depth of 165 m. The steep lee side of the ridges has an average slope gradient of 13° and a maximum of 26°, which show no relation with depth. In terms of wavelengths, the distance between the ridges is slightly more irregular than at the head of Martínez Channel and measures on average 105 m. Several gullies and remnant channel walls are visible along the channel. The unchannelized region on the upper delta slope also shows irregular bedforms consisting of sinuous scours and ridges. They cover a surface area of 1.7 km^2 and continue down to a depth of 115 m (Figs. 5b and 6c). Here, the ridges occur on a 5 to 10° slope.

Along the western shoreline of Steffen Fjord, a 7.5 km-long sinuous channel, with slightly elevated levees towards the central axis of the fjord, can be observed at the slope break (Figs. 5b and 6d). The maximum height difference between the bottom of the channel and the top of its levee is 18 m. Finally, a smaller subaquatic delta with a lobe-shaped fan is visible near a river inlet along the eastern shoreline of the fjord (Fig. 5b).

4.2. Sediment properties

4.2.1. Grain size

Mean sediment grain-size values at the head of Martínez Channel vary from 11.46 to 87.39 μm whereas samples from Steffen Fjord have mean grain-size values ranging from 6.09 to 411.66 μm. At the head of Martínez Channel, the majority of the samples are composed of fine to medium silt and most grain-size distributions are bimodal, whether the

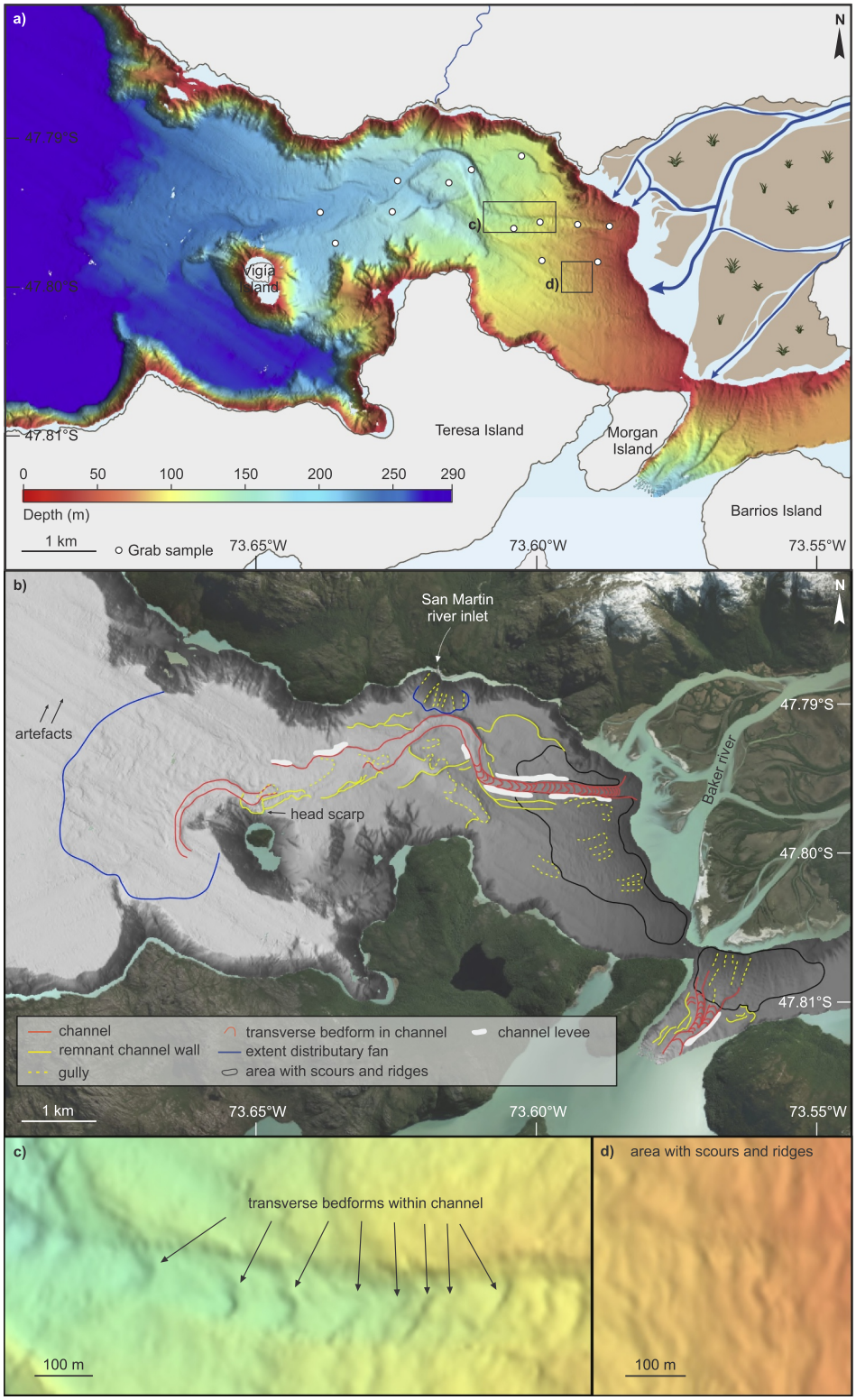

Fig. 3. Bathymetry of the Baker river delta and delta front at the head of Martínez Channel. (a) Bathymetric map and location of the grab sediment samples (white circles). (b) Grey shaded-relief bathymetry with indication of the main morphological features identified from the bathymetric data. (c) Enlargement of the transverse bedforms within the channel. (d) Enlargement of the non-channelized area with sinuous scours and ridges.

samples are from the channel or not (Fig. 7a and b). Samples located close to the delta lip are coarser and consist of coarse silt to fine sand. Likewise, samples situated near the delta margin of Steffen Fjord are slightly coarser (medium silt to medium sand) compared to samples further downslope (fine to medium silt) (Fig. 7c and d). In addition, the latter are better sorted compared to samples at the delta lip.

A clear difference in grain-size appears when comparing samples collected within the channels to samples from non-channelized regions, especially close to the shallow part of the deltas. As displayed in Fig. 7b (head of Martínez Channel) and 7d (Steffen Fjord), samples in the

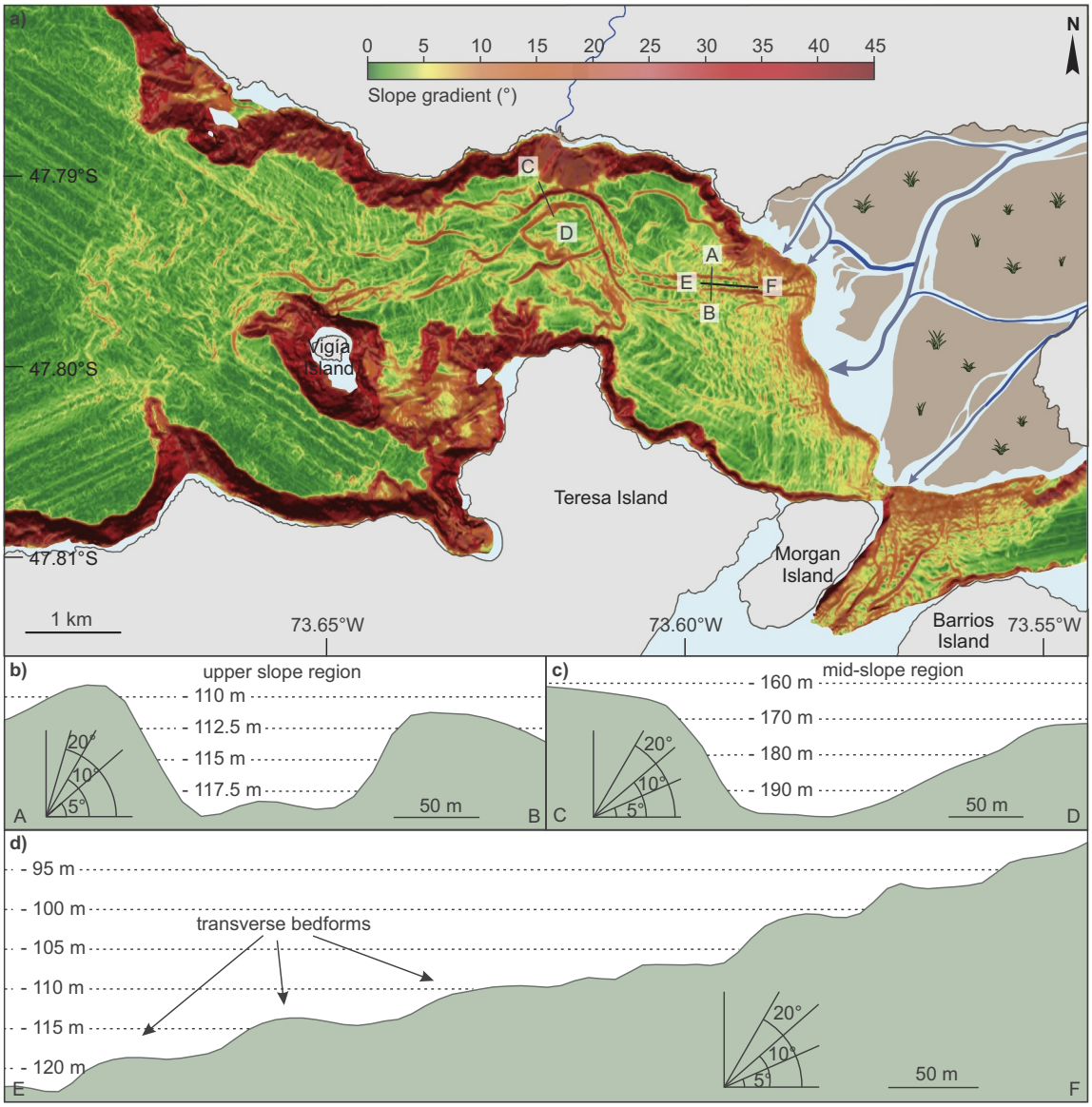

Fig. 4. (a) Slope map of the Baker river delta and prodelta at the head of Martínez Channel. (b–d) Cross-sections (see (a) for location) of the main channel in the upper slope region (b) and in the mid-slope area (c), and of the crescent-shaped transverse bedforms observed in the channel (d).

channels are consistently coarser compared to locations out of the channels at the same distance from the river mouth. To compare the amount of coarse particles between samples from the channel and from the non-channelized region, a boundary, i.e., the minimum between the two grain-size modes, was selected for both the head of Martínez Channel (14.5 μm) and Steffen Fjord (24.1 μm). This coarse particle percentage was calculated for each sample and is represented in Fig. 8. At both the head of Martínez Channel (Fig. 8a) and Steffen Fjord (Fig. 8b), results show a decreasing trend in the amount of coarse particles with increasing distance from the river mouths, and samples in the channels have consistently more coarse particles than samples outside of the channel, i.e., 44.3 versus 34.2% at the head of Martínez Channel and 24.6 versus 7.2% in Steffen Fjord.

4.2.2. Organic carbon content

Overall, TOC contents are low in both fjords, with average values higher at the head of Martínez Channel (0.56 ± 0.14%; Fig. 8c) than in Steffen Fjord (0.27 ± 0.07%; Fig. 8d). In Steffen Fjord, TOC does not vary with distance from the river mouth, depth, or location compared to the channel. In contrast, TOC values from the head of Martínez Channel display a general decreasing trend with depth, and they are systematically higher in the channels (0.61%) than in the non-channelized part of the delta (0.51%) (Fig. 8c).

5. Interpretation and discussion

5.1. Submarine channel systems

5.1.1. Channel activity

Channels at both the head of Martínez Channel and Steffen Fjord are deeply incised into their respective subaquatic deltas (Figs. 3 and 5). The presence of well-developed levees adjacent to the channels (Figs. 3b and 5b) implies recent channel activity, as the levees result from overspill during turbidity current activity within the channels. If the channels had not been active recently, these features would be buried under sediment settled from the surface plume and their morphology would become increasingly obscured. This is in agreement with the location of the channels in front of the river mouths, where large amounts of sediment is supplied to the fjords (Figs. 3 and 5).

Another clear indicator of recent channel activity is the presence of

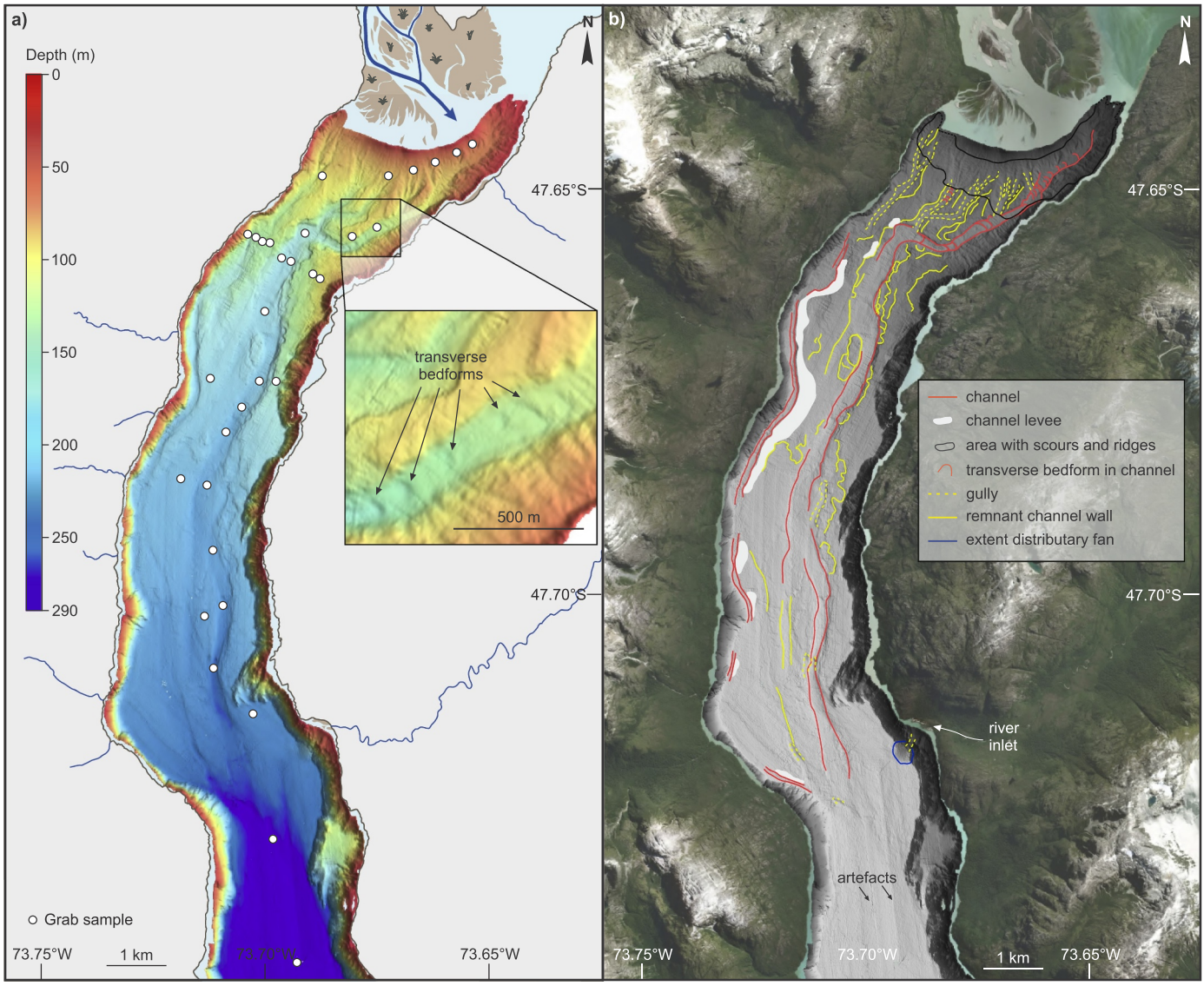

Fig. 5. Bathymetry of Steffen Fjord. (a) Grab sediment samples locations are indicated with white circles. The enlargement displays the transverse bedforms within the channel. (b) Grey shaded-relief bathymetry of Steffen Fjord with indication of the main morphological features identified from the bathymetric data.

crescent-shaped ridges within the axial channels of both the head of Martínez Channel and Steffen Fjord (Figs. 4d and 6c). These bedforms occur at similar depths (60–85 to 170–180 m) in both fjords (Figs. 3b and 5b), where the average slope is 2.9° for the head of Martínez Channel and 1.6° for Steffen Fjord. Such ridges, which are often referred to as sediment waves (e.g., Smith et al., 2005; Babonneau et al., 2013; Mazières et al., 2014; Dietrich et al., 2016; Normandeau et al., 2016b; Normandeau et al., 2019), are generally interpreted as a series of slowly migrating bedforms, where each lee side of the bedform is formed by a steeply dropping flow passing through a hydraulic jump before re-accelerating on the stoss side (Cartigny et al., 2011). They are regularly found in the proximal part of submarine channel systems, such as the Monterey Canyon in California (Paull et al., 2010), Canadian fjords (Prior et al., 1987; Conway et al., 2012; Normandeau et al., 2016a; Stacey and Hill, 2016), and the Fraser river delta (Hill, 2012). Depending on their geometry, internal structure, and grain-size distribution, channelized sediment waves can be classified into down-slope migrating (dunes) or up-slope migrating (cyclic steps, antidunes, chutes and pools) sediment waves (Cartigny et al., 2011). Channelized sediment waves with wavelengths and crest heights similar to those observed at the head of Martínez Channel and in Steffen Fjord have been interpreted as cyclic steps which migrate upslope and were hypothesized to be formed by supercritical dense underflows in the upper slope region (Hill, 2012; Babonneau et al., 2013; Hughes Clarke, 2016; Normandeau et al., 2016a; Stacey and Hill, 2016). The upslope orientation of the concave face of the sediment waves observed at the head of Martínez Channel and in Steffen Fjord suggests that the sediment waves are up-slope migrating cyclic steps (Hughes Clarke et al., 2012; Normandeau et al., 2016a; Stacey et al., 2018). In addition, the wavelengths of the bedforms at the head of Martínez Channel increase with distance from the delta margin. This indicates that due to decreasing slopes and increasing density flow specific discharge, the distance required for a turbidity current to return supercritical following a hydraulic jump increases (Fricke et al., 2015; Normandeau et al., 2016a). The latter might thus also explain why the distance between ridges increases downslope and ridges disappear in the lower slope region of the head of Martínez Channel and of Steffen Fjord. Compared to the well-developed ridges at the head of Martínez Channel, the ridges in Steffen Fjord are less pronounced and more irregular (Fig. 5). Given the recent retreat of Steffen Glacier and subsequent expansion of proglacial Steffen Lake (López and Casassa, 2011), turbidity current activity could have decreased in recent times due to the lake's filtering

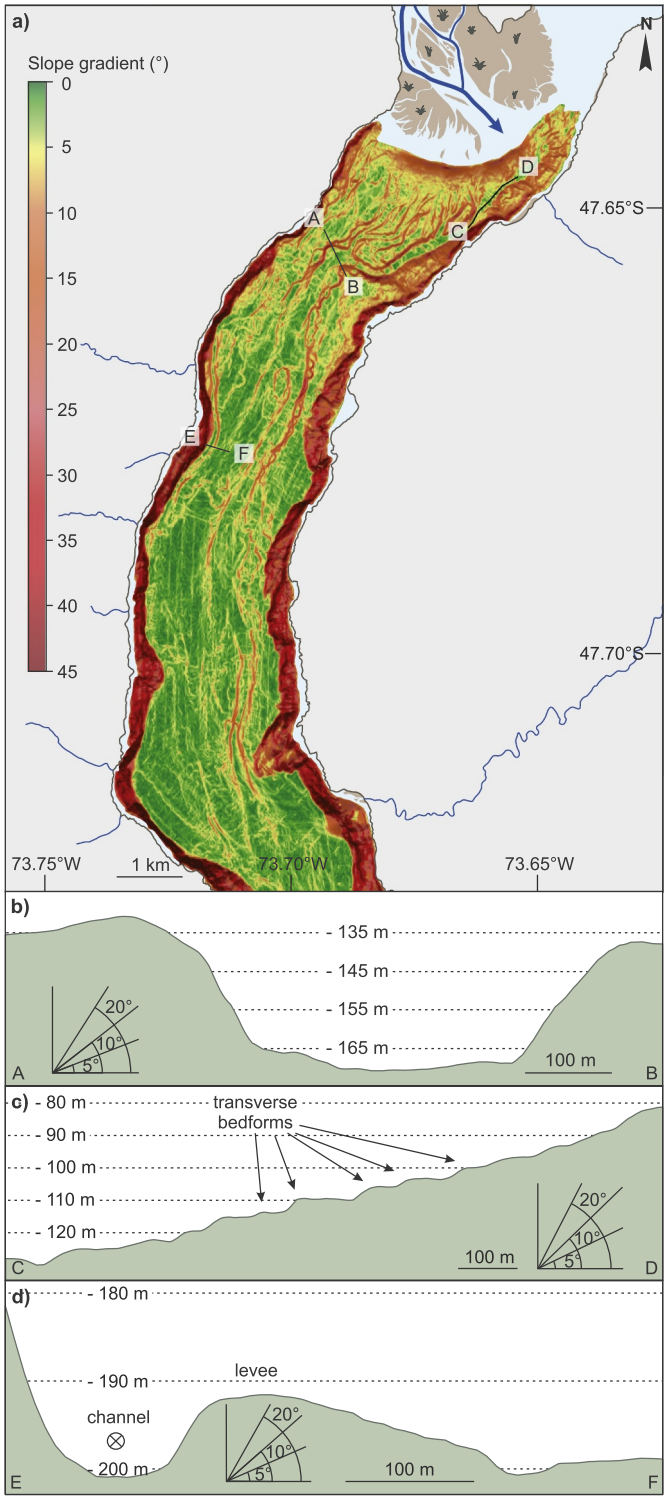

Fig. 6. (a) Slope map of Steffen Fjord. (b–d) Cross-sections (see (a) for location) through the main channel in the upper slope region (b), the crescent-shaped transverse bedforms observed within the channel (c), and the channel along the western shoreline (d).

effect (e.g., Normandeau et al., 2019). Finally, the steep slope angle of the Baker and Huemules river deltas promotes supercritical density flows, which is an additional argument for the up-slope migration of the ridges (Cartigny et al., 2011). Although the origin of channelized sediment waves is still debated, it is generally accepted that their formation involves flows at or close to the basin floor and can be associated with recent sediment transport (Wynn and Stow, 2002; Cartigny et al., 2011).

At the head of Martínez Channel, the presence of a head scarp north of Vigía Island (Fig. 3b) also implies recent channel activity. This scar feature represents a submarine slope failure which most likely occurred due to active scouring of the island's northern subaquatic slope by the channel. The absence of morphological evidence for landslide deposits within the channel and the observation that the channel is not yet buried implies the presence of eroding currents.

Recent channel activity at the head of Martínez Channel and in Steffen Fjord is additionally supported by data obtained on the grab sediment samples. Indeed, sediment within the channels is consistently coarser than in the non-channelized parts of the fjords and can thus be linked to a higher energetic environment (Figs. 7, 8a and b). It should however be noted that local variations in sediment grain size within the channels could also reflect the exact sampling location as sediments are generally coarser in the troughs than on the stoss of transverse bedforms (Postma and Cartigny, 2014). Although TOC values in Steffen Fjord are overall low due to the glacial nature of the sediment entering the fjord and do not show any significant difference between channels and the non-channelized region, samples from the head of Martínez Channel contain more organic matter, reflecting higher vegetation density in the watershed of Baker River. At the head of Martínez Channel, samples from the channels display higher TOC values compared to its non-channelized region due to the increased supply of terrestrial organic matter during periods of channel activity (Fig. 8c). The channels at the head of Martínez Channel and in Steffen Fjord can thus be interpreted as currently-active conduits for river sediment transport towards the deeper parts of the basinsFigs. 3 and 4.

The non-channelized region of the subaquatic deltas also displays sinuous-shaped scar features, but unlike the active channels, they do not cut deep into the subaquatic delta (Figs. 3b and 5b). These scars are most likely remnants of paleo-channels, which is supported by the relatively fine grain-size of the corresponding sediment samples in both fjords (Fig. 8a and b). These channels were probably abandoned during an intense turbidity event and subsequently buried by fine-grained sediment settling from the buoyant surface layer.

5.1.2. *Possible triggering mechanisms*

Subaquatic channel systems similar to those observed at the head of Martínez Channel and in Steffen Fjord have been described in many other regions such as the Chilean fjords adjacent to the SPI (Dowdeswell and Vásquez, 2013) and glaciofluvial fjords in the Northern Hemisphere (Prior et al., 1986; Syvitski et al., 1987; Conway et al., 2012; Hill, 2012; Stacey and Hill, 2016; Gales et al., 2019). They have also been identified in lake basins (Corella et al., 2016; Normandeau et al., 2016a) and on island slopes and continental margins (Wynn et al., 2002; Smith et al., 2005; Migeon et al., 2012; Babonneau et al., 2013).

In lake basins, most channel systems are related to turbidity currents forming at river mouths. In those systems, the density contrast between the inflowing sediment-laden water and the receiving freshwater basin favors sediment transport by turbidity currents (Mulder and Syvitski, 1995). These turbidity currents are a key factor in controlling the morphology of active channels (e.g., Corella et al., 2016) but they can also manifest as non-channelized undulating bedforms on the delta slope in the case of dilute and low density flows (e.g., Normandeau et al., 2016b). When rivers discharge into a fjord or marine system, on the other hand, coarse sediment is deposited on the delta slope and most fine particles propagate as a buoyant plume due to the strong salinity, temperature, and therefore density, stratification of the water column (Syvitski and Shaw, 1995). Still, turbidity currents can form in fjords due to either (a) repeated slope failures near the river inflow, or (b) discharge of relatively high suspended loads by rivers (Syvitski, 1989).

During slope failures at the delta front, sediment bodies can disintegrate and continue downslope as turbidity currents (Felix and Peakall,

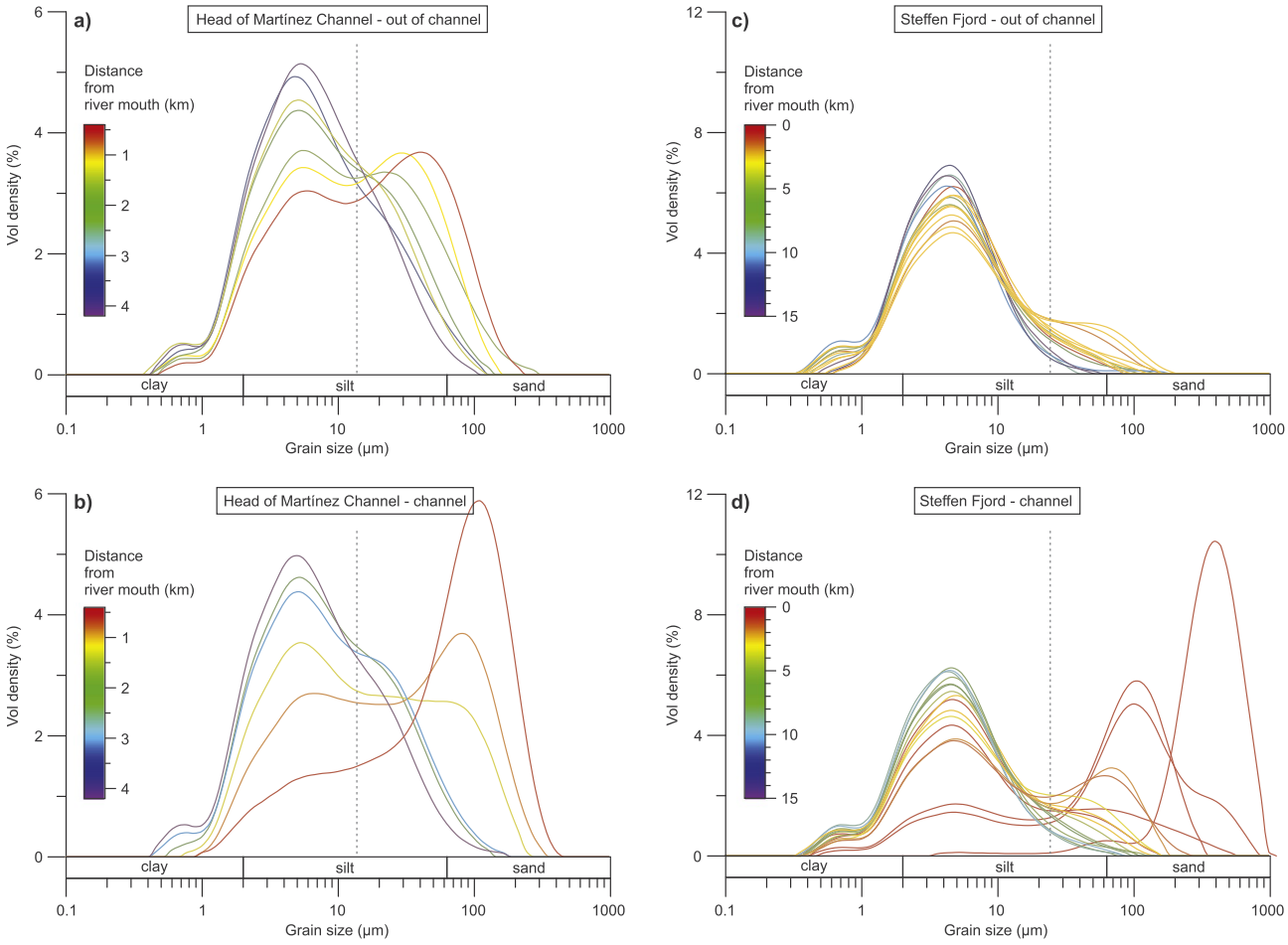

Fig. 7. Grain-size distribution of the grab sediment samples from the (a) non-channelized region and (b) channels at the head of Martínez Channel. (c–d) Same but for Steffen Fjord. Colors vary according to the distance from the river mouth. For Martínez Channel and Steffen Fjord, a grain-size boundary (inter-modal minimum) was set at 14.5 and 24.1 μm, respectively, to distinguish between the fine and coarse fractions (see also Fig. 8).

2006; Hughes Clarke et al., 2012). Several mechanisms can trigger submarine slope collapses, including sediment remobilization by seismic shaking, internal waves and/or tidal changes, and in case of organic-rich sediments, slides can also be triggered by the combination of tidal drawdown and gas compressibility effects (e.g., Smith et al., 1990). At the head of Martínez Channel and in Steffen Fjord, earthquake-triggered slope failure is considered unlikely since the study region is located just south of the Chile Triple Junction, in the so-called Patagonian Volcanic Gap, where seismic hazard is low compared to other regions along the Chilean coastline (Hayes et al., 2015). This is supported by the lack of registered earthquakes of magnitude $M > 3$ within 250 km of Tortel during the last 100 years (USGS earthquake catalog). Tidal drawdown processes are also considered unlikely due to the low tidal range (< 2 m) at the head of Martínez Channel and in Steffen Fjord compared to the Squamish Delta (British Columbia) and Sept-Îles (St-Lawrence Gulf), where tidal ranges of 3–5 m have been shown to result in sediment unloading (e.g., Clare et al., 2016; Dietrich et al., 2016). Tidal drawdown processes at the head of Martínez Channel and in Steffen Fjord might however be able to enhance slope failures during periods of peak discharge. Likewise, internal tides at the head of Martínez Channel appear to be correlated to high discharge pulses of Baker River (Ross et al., 2014), particularly in summer when river discharge exceeds 1200 m^3/s. Similar to tidal drawdown processes, internal tides occurring during periods of elevated river discharge might enhance slope failures but internal tides alone are likely not able to generate slope failures. Given the overall low TOC values in both fjords compared to other fjords where turbidity currents triggered by gas compression have been observed (Fraser Delta, Christian et al., 1997), gas compressibility is not considered a possible mechanism.

A far more likely mechanism for triggering turbidity currents at the heads of Martínez Channel and Steffen Fjord is the discharge of high suspended loads by Baker and Huemules rivers, respectively. Such a mechanism has been observed in the channel system of Bute Inlet (Canada), for example, where a large-scale turbidity event was associated with a major river flood due to heavy snowmelt (Prior et al., 1987). In other glaciofluvial dominated fjords in Canada, large-scale turbidity events responsible for the formation of submarine channels have also been related to river discharge peaks due to the rapid inflow of meltwater in summer (Conway et al., 2012; Hughes Clarke et al., 2012).

High discharge of sediment-laden river waters can create turbidity currents in fjords either directly (plunging of river waters, sediment settling from the river plume; Hizzett et al., 2018) or indirectly (rapid sediment accumulation at the delta-lip resulting in slope instability and eventually submarine slides). At the Squamish delta (British Columbia), for example, detailed monitoring revealed that delta-lip failures occurred with a delay of several hours after peak discharge due to cumulative sedimentation at the delta top and tidally-induced pore pressure changes (Clare et al., 2016). Delta slope failures seem to happen rather frequently to maintain maximum slope stability (Syvitski and Shaw, 1995). The plunging of river waters during floods represents a more direct hyperpycnal flow triggering mechanism (Mulder and Syvitski, 1995; Mulder et al., 2003). When sediment-laden river material entering the fjord is dense enough, it plunges and evolves into a

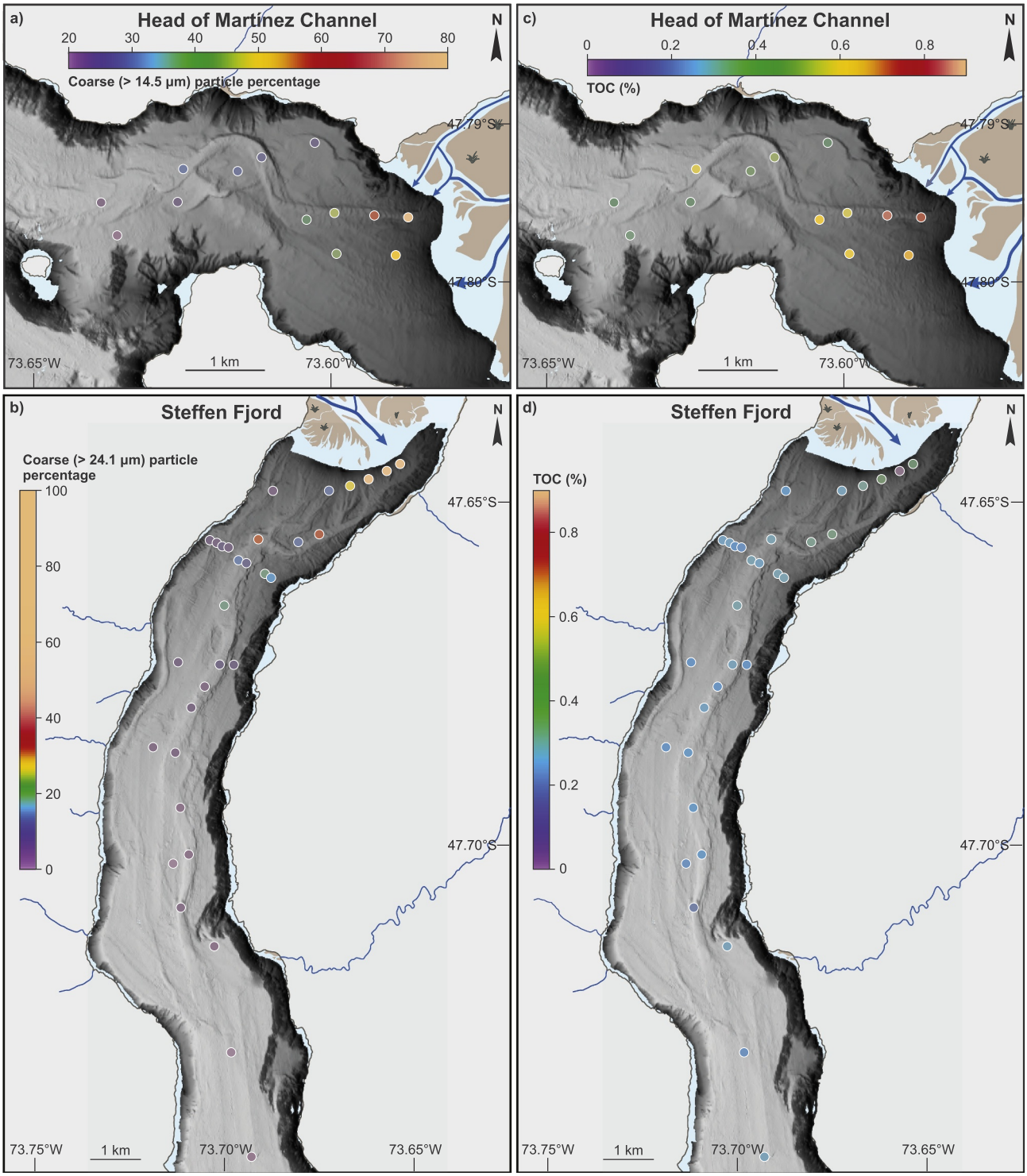

Fig. 8. Grain-size and organic carbon content in the delta region of the head of Martínez Channel and in Steffen Fjord. Coarse particle percentage of the grab sediment samples from (a) the head of Martínez Channel and (b) Steffen Fjord. (c–d) Same but for TOC. The grain-size boundaries used to calculate the coarse particle percentage were set at 14.5 and 24.1 µm for the head of Martínez Channel and Steffen Fjord, respectively (see Fig. 7 for rationale).

hyperpycnal flow (e.g., Dietrich et al., 2016). Finally, turbidity currents resulting from high suspended sediment loads, can also be triggered locally by sediment settling from the river plume (Parsons et al., 2001). These so-called "plume-triggered events" or "settling plume events" (Hizzett et al., 2018) are still poorly examined phenomena and only a few studies have described this process (e.g., Kineke et al., 2000; Hughes Clarke et al., 2014; Hizzett et al., 2018). Turbidity currents formed by plume-triggered events are more dilute compared to slope failures, and are able to maintain turbulence for longer periods of time, eventually leading to long runouts (Hizzett et al., 2018). At the Squamish delta (British Columbia), plume-triggered events dominate the triggering of underflows and contribute the majority of sediment to the depositional lobe, causing most of the seafloor changes on sub-annual timescales (Hizzett et al., 2018).

Theoretically, forming underflows in fjords requires suspended sediment concentrations of 30–40 g/l at the active river plume (Syvitski,

1989; Syvitski and Shaw, 1995) to overcome density contrasts between river water and sea water. Such high sediment concentrations have rarely been measured but flocculation within brackish waters has been suggested to enhance particle settling (Syvitski and Shaw, 1995), and experiments revealed that plume-triggered events can occur at sediment concentrations as low as 0.5 g/l (Parsons et al., 2001). At the Squamish delta (British Columbia) the recent results of Hage et al. (2019) even suggest that these plume-triggered events can be produced at sediment concentrations as low as 0.07 g/l, especially if they coincide with low tides.

Like other glaciofluvial fjord systems, the hydrography of Martínez Channel and Steffen Fjord is highly influenced by the hydrological cycle of inflowing rivers. During the melt season in summer, the discharge of Baker River doubles (DGA, Chile), and total suspended sediment concentrations reach on average 0.08 g/l (Supplementary Table A). Aside from seasonal increases, discharge and related suspended sediment concentrations can also peak during short-lived floods associated with either extreme precipitation (e.g., rain-on-snow events) or GLOFs. During GLOFs, suspended sediment concentrations in Baker River increase up to at least 0.78 g/l (Supplementary Table A), and water temperature drops by ~3 °C, causing a densification of the fjord surface waters near the river mouth.

The morphology of the subaquatic deltas described at the heads of Martínez Channel and Steffen Fjord resemble that of well-studied fjord systems in British Columbia (Gales et al., 2019), for which suspended sediment concentrations at the river outflow during the meltwater season ranges between 0.04 and 0.7 g/l. Monitoring studies show that the subaquatic channel systems of these deltas are highly active, especially during elevated river discharge in summer (Hage et al., 2018). In addition, the recent results of Hage et al. (2019) indicate that there may be no need for the suspended sediment to exceed a concentration threshold, which implies the possible generation of turbidity currents at a higher frequency than previously thought. By comparison with these well-studied systems, we posit that the channel systems identified at the head of Martínez Channel and in Steffen Fjord are also predominantly shaped by turbidity currents induced by elevated river discharge and the associated high amounts of suspended sediment. Such floods could include sporadic events during the meltwater season, rain-on-snow events, or GLOFs, and they may be able to trigger turbidity currents through direct plunging of the river plume or by the occurrence of plume-triggered events.

Deciphering between these three types of floods without detailed monitoring of river discharge and channel activity is almost impossible. The ability of GLOFs to trigger turbidity currents is particularly unclear at this stage due to the competing effects of high suspended sediment concentrations and low water temperature and salinity. On the one hand, suspended sediment concentrations measured during the GLOFs that occurred within the last 10 years are one order of magnitude higher than during the meltwater season (Supplementary Table A), which significantly increases water density. The increased meltwater input during GLOFs, on the other hand, increases fjord stratification, which may prevent the formation of hyperpycnal flows. GLOFs of the magnitude of those observed within the last decade may therefore not be able to trigger turbidity currents in the fjord. It is possible that only the extreme GLOFs, i.e., those with exceptional suspended sediment concentrations, are able to create turbidity currents, possibly resulting in channel migration.

One observation that seems to favor the occurrence of plume-triggered turbidity currents rather than direct plunging is the apparent lack of connection between the location of the head of the main (western) submarine channel at the head of Martínez Channel and that of the main Baker river channel (Fig. 3). Instead of being located immediately in front of the main present-day river branch, the submarine channel starts about 1.5 km to the north, suggesting that direct river plunging does not occur or is not able to carve deep subaquatic channels on the Baker river delta. This observation could however also reflect recent avulsion at the river mouth, which is supported by historical maps from the 1900s that show a better developed river channel on the northern side of the river delta (Nef, 1907; Supplementary Information Fig. B) immediately in front of the head of the subaquatic channel. The presence of abandoned channels on the subaquatic delta of Baker River may also reflect past avulsion (Fig. 3). The southern submarine channel being located immediately in front of the southern branch of Baker River (Fig. 3) supports this recent avulsion hypothesis. Such channel avulsions most likely occur during extreme discharge events, which have the potential to induce vigorous turbidity events, resulting in a complete re-organization of the subaquatic bedforms and channels (e.g., Kremer et al., 2015). Since very dilute river plumes are known to be able to trigger turbidity currents (Hage et al., 2019), this mechanism could explain our observations.

Taken together, the presence of turbidity currents carving channels through the deltas at the head of Martínez Channel and Steffen Fjord is most likely associated with elevated river discharge and with the associated input of high amounts of suspended sediments that occur during floods. Although detailed monitoring of the subaquatic deltas is required to investigate the exact triggering process(es), we expect plume-triggered events, and – to a lesser extent – direct plunging of the river plume, and/or slope failures at the delta lip enhanced by tidal drawdown processes and/or internal waves, to be the main geomorphic agents of the submarine delta at the head of Martínez Channel and Steffen Fjord.

5.2. Other morphological features

5.2.1. Along-slope channel in Steffen Fjord

The N-S oriented channel along the western shore of Steffen Fjord does not seem to be directly connected to the delta (Fig. 5b). Although it is interrupted at certain locations, this channel cuts deeply (up to 10 m) into the sediments at the bottom of the slope and recent activity is very likely given its clear morphology. The channel morphology also seems to be more pronounced at sharp turns along the shoreline, probably due to increasing flow velocity (Fig. 6d). There are two possible explanations for this channel feature. A first hypothesis is that it represents an abandoned turbidity channel and the associated levees. It could have been disconnected from the delta during a relatively recent major turbidity event. On the other hand, the along-slope channel geometry and the presence of 10-m high mounds along the eastern side of the channel tend to suggest its formation by bottom currents deflected by the western margin of the fjord, i.e., a sediment drift (Rebesco et al., 2014). Since the two-layer flow circulation of Steffen Fjord is composed of a hypopycnal cold brackish water surface layer flowing southwards underlain by a salty warmer layer of deeper Pacific Ocean water (Sievers and Silva, 2008; Moffat, 2014; Silva and Vargas, 2014), the bottom currents forming the sediment drift would most likely be directed northwards. Because this north-flowing bottom current originates at the outer fjord, it re-distributes fine-grained sediment, which explains why samples collected within this channel display grain-size values that are similar to the non-channelized areas (see the NW-SE grain-size transect in Fig. 8b). Due to the Coriolis effect, bottom currents flow parallel to the western steep fjord slope and the mounds are formed towards the central axis of the fjord, as currents are deflected counterclockwise. This effect might also be re-enforced by the prevailing westerly winds, which push surface waters towards the eastern side of the fjord, and therefore bottom waters towards the west.

Similar sediment drifts were described in lakes influenced by the southern westerlies, where they were interpreted as the result of wind-driven bottom currents (Gilli et al., 2005; Anselmetti et al., 2009; Heirman et al., 2012; Van Daele et al., 2016). However, both turbidity channels and sediment drifts result in very similar morphological features (e.g., mounded geometry) and it is not possible to identify the exact origin of this channel solely based on multibeam bathymetry.

5.2.2. Unchannelized sediment waves

Aside from the sediment waves within the axial channels, sinuous ridge and scour bedforms were also observed on the non-channelized deltas of both the head of Martínez Channel and Steffen Fjord. These features only occur on the upper slope, where gradients range from 5 to 15° (Figs. 3b and 5b). Similar bedforms have previously been observed at the Fraser delta (British Columbia), where they were interpreted as migrating sediment waves formed by unconfined turbidity currents on the delta slope (Hill, 2012). Other studies in lake basins have also linked the occurrence of non-channelized sediment waves on delta slopes, similar to those within the channels at the head of Martínez Channel and Steffen Fjord, to turbidity current activity (Normandeau et al., 2016a; Normandeau et al., 2016b). The sediment waves observed in the non-channelized upper flow regime of both the head of Martínez Channel and Steffen Fjord (Figs. 3–6), could therefore imply similar unconfined turbidity currents occurring on the delta slope. According to Howe et al. (2010), such sediment waves are an indicator of current reworking and bedload transport resulting from high sediment supply at river inflows in fjords.

In addition, the gullies observed in the non-channelized upper slope region at the head of Martínez Channel (Fig. 3b) also suggest the occurrence of high concentration turbidity currents (Syvitski et al., 1987). For example, the emplacement of cyclic steps on the upper foresets of a proglacial sandur delta were hypothesized to originate from river-derived hyperpycnal flows in a delta-front setting (Dietrich et al., 2016). The occurrence of unchannelized sediment waves at the head of Martínez Channel and Steffen Fjord is therefore an extra argument for non-channelized sediment migration or channel shifting due to the occurrence of large-scale turbidity events rather than slope failures.

5.2.3. Delta plain morphology: absence of moraines

Fjords are the product of glacial erosion. Therefore, fjord sediments generally preserve glaciomarine fans, and terminal and/or recessional moraines corresponding to glacier variations during the Quaternary (Howe et al., 2010). In Chilean fjords, Holocene moraines are generally well preserved (e.g., Rodrigo, 2008; Dowdeswell and Vásquez, 2013; Lastras and Dowdeswell, 2016). It is not surprising that no moraine features were observed at the head of Martínez Channel, since the fjord deglaciated over 8 kyr ago (Glasser et al., 2016). The lack of evidence of ice retreat in Steffen Fjord, however, is more surprising since the terminus of Steffen Glacier is located only 12 km landwards. The absence of a subaquatic moraine in Steffen Fjord supports the interpretation of Glasser et al. (2011) and Mardones et al. (2018) that Steffen Glacier remained land-based during the Little Ice Age advance. Neoglacial moraines could exist at the bottom of the fjord but would have been buried and are therefore no longer visible in the subaquatic morphology, as in other fjords of Chilean Patagonia (DaSilva et al., 1997; Moffat, 2014; Piret et al., 2017b). Given the depth of the fjord, it is also possible that Steffen Glacier was calving, instead of grounded, which could also explain the absence of subaquatic moraines in Steffen Fjord.

5.3. Implications for paleoclimate and paleoenvironmental research: site selection

The presence of channels actively carving through the deltas at the head of Martínez Channel and Steffen Fjord has important implications for the selection of coring sites for future paleoclimate and paleoenvironmental research. Our results show that the processes of sediment transport and deposition at the head of these fjords can vary within a few hundreds of meters, which makes proper site selection crucial. In both fjords, the channels act as conduits for the transport of relatively coarse river sediments to the prodelta areas. At these locations, sediment preservation is expected to be very low due to strong erosional processes (e.g., Vendettuoli et al., 2019). This implies that ideal coring sites for paleohydrological reconstructions (extreme events) should be located on the distal fan lobe, out of the channel axis. It should however be noted that sedimentation in the distal region of river/delta systems dominated by subaquatic channels is directly linked to the activity of the channels, i.e. the location of the river mouth and the delta slope morphology (Kremer et al., 2015). Channel shifts at the head of Martínez Channel and in Steffen Fjord, which are very likely to have occurred in the past, can thus result in significant lithological variations and caution should be exercised when interpreting long sediment records in terms of past flood occurrence. To account for channel migration, a multi-core approach, and possibly the acquisition of seismic data, are recommended. At distal locations, large floods are expected to be recorded as turbidites intercalated within finer sediment settling from the surficial plume. Sites located closer to the delta will likely register more floods compared to sampling sites further away, which will only contain evidence of the largest or most extreme events.

6. Conclusions

High-resolution bathymetric imagery of the heads of Martínez Channel and Steffen Fjord reveal that the fjords' morphology is characterized by large subaquatic deltas incised by up-to-36 m deep submarine channels. The presence of these channels, together with the occurrence of channelized sediment waves and coarser sediments within the channels, reflect recent sediment transport by turbidity currents. Although detailed monitoring is required to pinpoint the exact triggering mechanism(s) of the turbidity currents in these two fjords, we argue that these currents are related to periods of elevated discharge of Baker and Huemules rivers and to the associated high suspended sediment loads, irrespective of the flood's origin (seasonal increase, high precipitation event, or GLOFs). These turbidity currents are most likely formed by plume-triggered events and to a lesser extent by direct plunging of the river plume, and/or slope failures at the delta lip, potentially enhanced by tidal drawdown processes and/or internal waves. Increased river discharge during meltwater events, GLOFs, and intense precipitation are hypothesized to be of key importance in shaping the submarine channels and thus the geomorphology of the heads of Martínez Channel and Steffen Fjord. Our results also highlight the importance of high-resolution bathymetric mapping before any sediment coring activities. Avoiding blind coring is especially important at fjord heads, where delta morphology is highly influenced by active channel processes. Future sediment-based paleoclimate and paleoenvironmental reconstructions at the head of Martínez Channel and in Steffen Fjord should therefore highly benefit from the bathymetric map presented in this paper.

Data availability

The bathymetric map related to this article can be found on Marine Geoscience Data System (MGDS; DOIs10.1594/IEDA/324731, 324732, 324733, 324734).

Declaration of competing interest

The authors declare that they have no known competing financial interests or personal relationships that could have appeared to influence the work reported in this paper.

Acknowledgements

We thank Koen De Rycker, Helena Pryer, Loïc Piret, and Fernando Torrejón for their help with data acquisition and sample collection. We are also thankful to the captain (Rodrigo Mansilla) and crew of the *R/V Sur-Austral* (COPAS Sur-Austral, Tortel, Chile), and to the staff of Centro de Investigación en Ecosistemas de la Patagonia (CIEP, Chile). We wish to thank Romina San Martín (University of Concepción, Chile) for easing the administration and Carlos Moffat (University of Delaware, USA) for providing the tide files. Philipp Kempf, Thomas Vandorpe, and

Nore Praet are thanked for their help with data processing. The Flanders Marine Institute (VLIZ) is acknowledged for providing the *Caris* software and QPS is thanked for the academic discount on the *Fledermaus* software. Finally, we acknowledge the Chilean Navy Hydrographic and Oceanographic Service (SHOA) for the authorization to map the fjords (permit number 13270/24/235/Vrs). The research presented here was funded by the Flemish Research Foundation (FWO, Belgium) Paleo-GLOFs project G0D7916N and by UGent BOF project HYDROPROX (01 N02216). We are grateful to Loïc Piret and Benjamin Amann for commenting on an earlier version of this manuscript. The authors wish to thank three anonymous reviewers for their constructive comments that improved this manuscript.

Appendix A. Supplementary data

Supplementary data to this article can be found online at https://doi.org/10.1016/j.margeo.2019.106076.

References

Aniya, M., 2014. GLOF of a side-lake, Laguna de los Témpanos, of Glaciar Steffen, Hielo Patagónico Norte, South America (in Japanese). In: Proceedings of JSSI & JSSE Joint Conference – 2014/Hachinohe. pp. A1–A7.

Anselmetti, F.S., Ariztegui, D., De Batist, M., Gebhardt, A.C., Haberzettl, T., Niessen, F., Ohlendorf, C., Zolitschka, B., 2009. Environmental history of southern Patagonia unravelled by the seismic stratigraphy of Laguna Potrok Aike. Sedimentology 56, 873–892. https://doi.org/10.1111/j.1365-3091.2008.01002.x.

Araya Vergara, J.F., 2011. Submarine failures in the bottom of the Aysén fjord, Northern Patagonia, Chile. Investig. Geogr. 43, 17–34.

Babonneau, N., Delacourt, C., Cancouët, R., Sisavath, E., Bachèlery, P., Mazuel, A., Jorry, S.J., Deschamps, A., Ammann, J., Villeneuve, N., 2013. Direct sediment transfer from land to deep-sea: Insights into shallow multibeam bathymetry at La Réunion Island. Mar. Geol. 346, 47–57. https://doi.org/10.1016/j.margeo.2013.08.006.

Bastianon, E., Bertoldi, W., Dussaillant, A., 2012. Glacial-lake outburst flood effects on Colonia River morphology, Chilean Patagonia. In: River Flow. 2012. CRC Press, pp. 573–579.

Bertrand, S., Hughen, K.A., Lamy, F., Stuut, J.-B.W., Torrejón, F., Lange, C.B., 2012. Precipitation as the main driver of Neoglacial fluctuations of Gualas glacier, Northern Patagonian Icefield. Clim. Past 8, 519–534. https://doi.org/10.5194/cp-8-519-2012.

Bertrand, S., Hughen, K., Sepúlveda, J., Pantoja, S., 2014. Late Holocene covariability of the southern westerlies and sea surface temperature in northern Chilean Patagonia. Quat. Sci. Rev. 105, 195–208. https://doi.org/10.1016/j.quascirev.2014.09.021.

Bertrand, S., Lange, C.B., Pantoja, S., Hughen, K., Van Tornhout, E., Smith Wellner, J., 2017. Postglacial fluctuations of Cordillera Darwin glaciers (southernmost Patagonia) reconstructed from Almirantazgo fjord sediments. Quat. Sci. Rev. 177, 265–275. https://doi.org/10.1016/j.quascirev.2017.10.029.

Boyd, B.L., Anderson, J.B., Wellner, J.S., Fernández, R.A., 2008. The sedimentary record of glacial retreat, Marinelli Fjord, Patagonia: Regional correlations and climate ties. Mar. Geol. 255, 165–178. https://doi.org/10.1016/l.margeo.2008.09.001.

Caldenius, C.C., 1932. Las glaciaciones cuaternarios en la Patagonia y Tierra del Fuego. Geogr. Ann. 14, 144–157.

Caniupán, M., Lamy, F., Lange, C., Kaiser, J., Kilian, R., Arz, H.W., León, T., Mollenhauer, G., Sandoval, S., De Pol-Holz, R., Pantoja, S., Wellner, J., Tiedemann, R., 2014. Holocene sea-surface temperature variability in the Chilean fjord region. Quat. Res. 82, 342–353.

Cartigny, M.J.B., Postma, G., van den Berg, J.H., Mastbergen, D.R., 2011. A comparative study of sediment waves and cyclic steps based on geometries, internal structures and numerical modeling. Mar. Geol. 280, 40–56.

Clare, M.A., Hughes Clarke, J.E., Talling, P.J., Cartigny, M.J.B., Pratomo, D.G., 2016. Preconditioning and triggering of offshore slope failures and turbidity currents revealed by most detailed monitoring yet at a fjord-head delta. Earth Planet. Sci. Lett. 450, 208–220.

Conway, K.W., Barrie, J.V., Picard, K., Bornhold, B.D., 2012. Submarine channel evolution: active channels in fjords, British Columbia, Canada. Geo-Mar. Lett. 32, 301–312.

Corella, J.P., Loizeau, J.-L., Kremer, K., Hilbe, M., Gerard, J., le Dantec, N., Stark, N., González-Quijano, M., Girardclos, S., 2016. The role of mass-transport deposits and turbidites in shaping modern lacustrine deepwater channels. Mar. Pet. Geol. 77, 515–525.

Christian, H.A., Mosher, D.C., Mulder, T., Barrie, J.V., Courtney, R.C, 1997. Geomorphology and potential slope instability on the Fraser River delta foreslope, Vancouver, British Columbia. Canadian Geotechnical Journal 34, 432–446.

DaSilva, J.L., Anderson, J.B., Stravers, J., 1997. Seismic facies changes along a nearly continuous 24° latitudinal transect: the fjords of Chile and the northern Antarctic Peninsula. Mar. Geol. 143, 103–123.

Davies, B.J., Glasser, N.F., 2012. Accelerating shrinkage of Patagonian glaciers from the Little Ice Age (~AD 1870) to 2011. J. Glaciol. 58 (212), 1063–1084.

DGA, 2019. Minuta Tecnica N° 1, 22 de enero de 2019, Inundación río Huemules Superior, sector Estero Steffen. (7 p).

Dietrich, P., Ghienne, J.-F., Normandeau, A., Lajeunesse, P., 2016. Upslope-migrating bedforms in a proglacial sandur delta: cyclic steps from river-derived underflows. J. Sediment. Res. 86, 112–122.

Douglass, D.C., Singer, B.S., Kaplan, M.R., Ackert, R.P., Mickelson, D.M., Caffee, M.W., 2005. Evidence of early Holocene glacial advances in southern South America from cosmogenic surface-exposure dating. Geology 33 (3), 237–240.

Dowdeswell, J.A., Vásquez, M., 2013. Submarine landforms in the fjords of southern Chile: implications for glacimarine processes and sedimentation in a mild glacier-influenced environment. Quat. Sci. Rev. 64, 1–19.

Dussaillant, A., Benito, G., Buytaert, W., Carling, P., Meier, C., Espinoza, F., 2010. Repeated glacial-lake outburst floods in Patagonia: an increasing hazard? Nat. Hazards 54, 469–481. https://doi.org/10.1007/s11069-009-9479-8.

Felix, M., Peakall, J., 2006. Transformation of debris flows into turbidity currents: mechanisms inferred from laboratory experiments. Sedimentology 53 (1), 107–123. https://doi.org/10.1111/j.1365-3091.2005.00757.x.

Fricke, A.T., Sheets, B.A., Nittrouer, C.A., Allison, M.A., Ogston, A.S., 2015. An examination of Froude-supercritical flows and cyclic steps on a subaqueous lacustrine delta, Lake Chelan, Washington, U.S.A. J. Sediment. Res. 85, 754–767.

Gales, J.A., Talling, P.J., Cartigny, M.J.B., Hughes Clarke, J., Lintern, G., Stacey, C., Clare, M.A., 2019. What controls submarine channel development and the morphology of deltas entering deep-water fjords? Earth Surf. Process. Landf. 44, 535–551. https://doi.org/10.1002/esp.4515.

García, J.L., Kaplan, M.R., Hall, B.L., Schaefer, J.M., Vega, R.M., Schwartz, R., Finkel, R., 2012. Glacier expansion in southern Patagonia throughout the Antarctic cold reversal. Geology 40, 859–862.

Gilli, A., Anselmetti, F.S., Ariztegui, D., Beres, M., McKenzie, J.A., Markgraf, V., 2005. Seismic stratigraphy, buried beach ridges and contourite drifts: the Late Quaternary history of the closed Lago Cardiel basin, Argentina (49 °S). Sedimentology 52, 1–23. https://doi.org/10.1111/j.1365-3091.2004.00677.x.

Glasser, N.F., Harrison, S., Jansson, K.N., Anderson, K., Cowley, A., 2011. Global sea-level contribution from the Patagonian Icefields since the Little Ice Age maximum. Nat. Geosci. 4, 303–307.

Glasser, N.F., Harrison, S., Schnabel, C., Fabel, D., Jansson, K.N., 2012. Younger Dryas and early Holocene age glacier advances in Patagonia. Quat. Sci. Rev. 58, 7–17.

Glasser, N.F., Jansson, K.N., Duller, G.A.T., Singarayer, J., Holloway, M., Harrison, S., 2016. Glacial lake drainage in Patagonia (13-8 kyr) and response of the adjacent Pacific Ocean. Sci. Rep. 6, 21064. https://doi.org/10.1038/srep21064.

Hage, S., Cartigny, M.J.B., Clare, M.A., Sumner, E.J., Vendettuoli, D., Hughes Clarke, J.E., Hubbard, S.M., Talling, P.J., Lintern, D.G., Stacey, C.D., Englert, R.G., Vardy, M.E., Hunt, J.E., Yokokawa, M., Parsons, D.R., Hizzett, J.L., Azpiroz-Zabala, M., Vellinga, A.J., 2018. How to recognize crescentic bedforms formed by supercritical turbidity currents in the geologic record: Insights from active submarine channels. Geology 46, 563–566.

Hage, S., Cartigny, M.J.B., Sumner, E.J., Clare, M.A., Hughes Clarke, J.E., Talling, P.J., Lintern, D.G., Simmons, S.M., Silva Jacinto, R., Vellinga, A.J., Allin, J.R., Azpiroz-Zabala, M., Gales, J.A., Hizzett, J.L., Hunt, J.E., Mozzato, A., Parsons, D.R., Pope, E.L., Stacey, C.D., Symons, W.O., Vardy, M.E., Watts, C., 2019. Direct monitoring reveals initiation of turbidity currents from extremely dilute river plumes. Accepted for publication. Geophys. Res. Lett. https://doi.org/10.1029/2019GL084526.

Harrison, S., Glasser, N.F., 2011. The Pleistocene glaciations of Chile. In: Ehlers, J., Gibbard, P.L., Hughes, P.D. (Eds.), Quaternary Glaciations – Extent and Chronology – A Closer Look. Developments in Quaternary Sciences, vol. 15. Elsevier, Amsterdam, pp. 739–756.

Harrison, S., Winchester, V., Glasser, N., 2007. The timing and nature of recession of outlet glaciers of Hielo Patagónico Norte, Chile, from their Neoglacial IV (Little Ice Age) maximum positions. Glob. Planet. Chang. 59, 67–78.

Hayes, G.P., Smoczyk, G.M., Benz, H.M., Villaseñor, A., Furlong, K.P., 2015. Seismicity of the Earth 1900–2013, Seismotectonics of South America (Nazca Plate Region): U.S. Geological Survey Open-File Report 2015–1031-E, 1 Sheet, Scale 1:14 000 000. https://doi.org/10.3133/of20151031E.

Heirman, K., De Batist, M., Arnaud, F., De Beaulieu, J.-L., 2012. Seismic stratigraphy of the late Quaternary sedimentary infill of Lac d'Armor (Kerguelen archipelago): a record of glacier retreat, sedimentary mass wasting and southern Westerly intensification. Antarct. Sci. 24, 608–618. https://doi.org/10.1017/S0954102012000466.

Hill, P.R., 2012. Changes in submarine channel morphology and slope sedimentation patterns from repeat multibeam surveys in the Fraser River delta, western Canada. Int. Assoc. Sedimentol. Spec. Publ. 44, 47–70.

Hizzett, J.L., Hughes Clarke, J.E., Sumner, E.J., Cartigny, M.J.B., Talling, P.J., Clare, M.A., 2018. Which triggers produce the most erosive, frequent, and longest runout turbidity currents on deltas? Geophys. Res. Lett. 45 (2), 855–863.

Howe, J.A., Austin, W.E.N., Forwick, M., Paetzel, M., Harland, R., Cage, A.G., 2010. Fjord systems and archives: a review. In: Howe, J.A., Austin, W.E.N., Forwick, M., Paetzel, M. (Eds.), Fjord Systems and Archives. Geological Society, London, Special Publications 344. pp. 5–15. https://doi.org/10.1144/SP344.2.

Hubbard, A., Hein, A.S., Kaplan, M.R., Hulton, N.R.J., Glasser, N., 2005. A modelling reconstruction of the Last Glacial Maximum Ice Sheet and its deglaciation in the vicinity of the Northern Patagonian Icefield, South America. Geogr. Ann. 87 A (2), 375–391.

Hughes Clarke, J.E., 2016. First wide-angle view of channelized turbidity currents links migrating cyclic steps to flow characteristics. Nat. Commun. 7, 11896. https://doi.org/10.1038/ncomms11896.

Hughes Clarke, J.E., Brucker, S., Muggah, J., Hamilton, T., Cartwright, D., Church, I., Kuus, P., 2012. Temporal progression and spatial extent of mass wasting events on the Squamish prodelta slope. In: Landslides and Engineered Slopes: Protecting Society through Improved Understanding, vol. 122. Taylor and Francis Group, London, pp. 1091–1096.

Hughes Clarke, J.E., Marques, C.R.V., Pratomo, D., 2014. Imaging Active Mass-Wasting

and Sediment Flows on a Fjord Delta. Springer International Publishing, Squamish, British Columbia, pp. 249–260.
Iriarte, J.L., Pantoja, S., Daneri, D., 2014. Oceanographic processes in Chilean fjords of Patagonia: from small to large-scale studies. Prog. Oceanogr. 129, 1–7.
Jacquet, J., McCoy, S.W., McGrath, D., Nimick, D.A., Fahey, M., O'kuinghttons, J., Friesen, B.A., Leidlich, J., 2017. Hydrologic and geomorphic changes resulting from episodic glacial lake outburst floods: Rio Colonia, Patagonia, Chile. Geophys. Res. Lett. 44, 854–864. https://doi.org/10.1002/2016GL071374.
Kaplan, M.R., Ackert Jr., R.P., Singer, B.S., Douglass, D.C., Kurz, M.D., 2004. Cosmogenic nuclide chronology of millennial-scale glacial advances during O-isotope stage 2 in Patagonia. Geol. Soc. Am. Bull. 116 (3/4), 308–321.
Kineke, G.C., Woolfe, K.J., Kuehl, S.A., Milliman, J.D., Dellapenna, T.M., Purdon, R.G., 2000. Sediment export from the Sepik River, Papua New Guinea: evidence for a divergent sediment plume. Cont. Shelf Res. 20, 2239–2266.
Kremer, K., Corella, J.P., Hilbe, M., Marillier, F., Dupuy, D., Zenhäusern, G., Girardclos, S., 2015. Changes in distal sedimentation regime of the Rhone delta systems controlled by subaquatic channels (Lake Geneva, Switzerland/France). Mar. Geol. 370, 125–135.
Lamy, F., Kilian, R., Arz, H.W., Francois, J.-P., Kaiser, J., Prange, M., Steinke, T., 2010. Holocene changes in the position and intensity of the southern westerly wind belt. Nat. Geosci. 3, 695–699.
Lastras, G., Dowdeswell, J.A., 2016. Terminal and recessional moraines in the fjords of southern Chile. In: Dowdeswell, J.A., Canals, M., Jakobsson, M., Todd, B.J., Dowdeswell, E.K., Hogan, E.K. (Eds.), Atlas of Submarine Glacial Landforms: Modern, Quaternary and Ancient. Geological Society, London, Memoirs 46. pp. 65–66.
Lliboutry, L., 1965. Nieves y Glaciars de Chile, fundamento de glaciologia, Chile. Ediciones de la Universidad de Chile (417 pp).
López, P., Casassa, G., 2011. Recent acceleration of ice loss in the Northern Patagonian Icefield. Cryosphere Discuss. 5, 3323–3381.
Lopez, P., Chevallier, P., Favier, V., Pouyaud, B., Ordenes, F., Oerlemans, J., 2010. A regional view of fluctuations in glacier length in southern South America. Glob. Planet. Chang. 71, 85–108.
Mardones, M., Aguayo, M.A., Smith, E.A., Ruiz, P.L., 2018. Retroceso glacial reciente en al Campo de Hielo Norte, región de Aysén: relación con variaciones climáticas. Rev. Geogr. Norte Grande (69), 121–147.
Marin, V.H., Tironi, A., Paredes, M.A., Contreras, M., 2013. Modeling suspended solids in a Northern Chilean Patagonia glacier-fed fjord: GLOF scenarios under climate change conditions. Ecol. Model. 264, 7–16. https://doi.org/10.1016/j.ecolmodel.2012.06.017.
Mazières, A., Gillet, H., Castelle, B., Mulder, T., Guyot, C., Garlan, T., Mallet, C., 2014. High-resolution morphobathymetric analysis and evolution of Capbreton submarine canyon head (Southeast Bay of Biscay – French Atlantic Coast) over the last decade using descriptive and numerical modeling. Mar. Geol. 351, 1–12.
Meerhoff, E., Castro, L.R., Tapia, F.J., Pérez-Santos, I., 2018. Hydrographic and biological impacts of a Glacial Lake Outburst Flood (GLOF) in a Patagonian fjord. Estuar. Coasts 42, 132–143. https://doi.org/10.1007/s12237-018-0449-9.
Migeon, S., Mulder, T., Savoye, B., Sage, F., 2012. Hydrodynamic processes, velocity structure and stratification in natural turbidity currents: results inferred from field data in the Var Turbidite System. Sediment. Geol. 245-246, 48–62.
Moffat, C., 2014. Wind-driven modulation of warm water supply to a proglacial fjord, Jorge Montt Glacier, Patagonia. Geophys. Res. Lett. 41, 3943–3950.
Mulder, T., Syvitski, J.P.M., 1995. Turbidity currents generated at river mouths during exceptional discharges to the world oceans. J. Geol. 103, 285–299.
Mulder, T., Syvitski, J.P.M., Migeon, S., Faugères, J.-C., Savoye, B., 2003. Marine hyperpycnal flows: initiation, behavior and related deposits. A review. Mar. Pet. Geol. 20, 861–882.
Nef, F., 1907. Estuario Canal Baker, 1:200000, Chile.
Normandeau, A., Lajeunesse, P., Poiré, A.G., Francus, P., 2016a. Morphological expression of bedforms formed by supercritical sediment density flows on four fjord-lake deltas of the south-eastern Canadian Shield (Eastern Canada). Sedimentology 63, 2106–2129.
Normandeau, A., Lamoureux, S.F., Lajeunesse, P., Francus, P., 2016b. Sediment dynamics in paired High Arctic lakes revealed from high-resolution swath bathymetry and acoustic stratigraphy surveys. J. Geophys. Res. Earth 121, 1676–1696.
Normandeau, A., Dietrich, P., Hughes Clarke, J., Van Wychen, W., Lajeunesse, P., Burgess, D., Ghienne, J.-F., 2019. Retreat pattern of glaciers controls the occurrence of turbidity currents on high-latitude fjord deltas (eastern Baffin Island). J. Geophys. Res. Earth 124, 1559–1571 (accepted).
Parsons, J.D., Bush, J.W.M., Syvitski, J.P.M., 2001. Hyperpycnal plume formation from riverine outflows with small sediment concentrations. Sedimentology 48, 465–478.
Paull, C.K., Ussler III, W., Caress, D.W., Lundsten, E., Covault, J.A., Maier, K.L., Xu, J., Augenstein, S., 2010. Origins of large crescent-shaped bedforms within the axial channel of Monterey Canyon, offshore California. Geosphere 6, 755–774.
Piret, L., Bertrand, S., Kissel, C., De Pol-Holz, R., Tamayo Hernando, A., Van Daele, M., 2017a. First evidence of a mid-Holocene earthquake-triggered megaturbidite south of the Chile Triple Junction. Sediment. Geol. 375, 120–133. https://doi.org/10.1016/j.sedgeo.2018.01.002.
Piret, L., Bertrand, S., Vandekerkhove, E., Harada, N., Moffat, C., Rivera, A., 2017b. Gridded bathymetry of the Baker-Martinez fjord complex (Chile, 48°S) v1. Figshare. Fileset. https://doi.org/10.6084/m9.figshare.5285521.v3.
Postma, G., Cartigny, J.B., 2014. Supercritical and subcritical turbidite currents and their deposits – a synthesis. Geology 42, 987–990. https://doi.org/10.1130/G35957.
Prior, D.B., Bornhold, B.D., Johns, M.W., 1986. Active sand transport along a fjord-bottom channel, Bute Inlet, British Colombia. Geology 14, 581–584.
Prior, D.B., Bornhold, B.D., Wiseman, W.J., Lowe Jr., D.R., 1987. Turbidity current activity in a British Columbia fjord. Science 237, 1330–1333.
Quiroga, E., Ortiz, P., Gerdes, D., Reid, B., Villagran, S., Quiñones, R., 2012. Organic enrichment and structure of macrobenthic communities in the glacial Baker fjord, Northern Patagonia, Chile. J. Mar. Biol. Assoc. U. K. 92 (1), 73–83.
Rebesco, M., Hernández-Molina, F.J., Van Rooij, D., Wåhlin, A., 2014. Contourites and associated sediments controlled by deep-water circulation processes: State-of-the-art and future considerations. Marine Geology 352, 111–154.
Rodrigo, C., 2008. Submarine topography in the Chilean North Patagonian channels. In: Silva, N., Palma, S. (Eds.), Progress in the Oceanographic Knowledge of Chilean Interior Waters, From Puerto Montt to Cape Horn. Comité Oceanográfico Nacional – Pontificia Universidad Católica de Valparaíso, Valparaíso, pp. 19–23.
Ross, L., Pérez-Santos, I., Valle-Levinson, A., Schneider, W., 2014. Semidiurnal internal tides in a Patagonian fjord. Prog. Oceanogr. 129, 19–34.
Sepúlveda, J., Pantoja, S., Hughen, K.A., Bertrand, S., Figueroa, D., León, T., Drenzek, N.J., Lange, C., 2009. Late Holocene sea-surface temperature and precipitation variability in northern Patagonia, Chile (Jacaf Fjord, 44°S). Quat. Res. 72, 400–409.
Servicio Hidrográfico y Oceanográfico de la Armada, 2001. Canal Baker, 6th edition. (1:200000, Valparaíso, Chile).
Sievers, H.A., Silva, N., 2008. Water masses and circulation in austral Chilean channels and fjords. In: Silva, N., Palma, S. (Eds.), Progress in the Oceanographic Knowledge of Chilean Interior Waters, From Puerto Montt to Cape Horn. Comité Oceanográfico Nacional – Pontificia Universidad Católica de Valparaíso, Valparaíso, pp. 53–58.
Silva, N., Vargas, C.A., 2014. Hypoxia in Chilean Patagonian Fjords. Prog. Oceanogr. 129, 62–74. https://doi.org/10.1016/j.pocean.2014.05.016.
Smith, N.D., Phillips, A.C., Powell, R.D., 1990. Tidal drawdown: a mechanism for producing cyclic sediment laminations in glaciomarine deltas. Geology 18, 10–13.
Smith, D.P., Ruiz, G., Kvitek, R., Iampietro, P.J., 2005. Semiannual patterns of erosion and deposition in upper Monterey Canyon from serial multibeam bathymetry. GSA Bull. 117, 1123–1133. https://doi.org/10.1130/B25510.1.
Stacey, C.D., Hill, P.R., 2016. Cyclic steps on a glacifluvial delta, Howe Sound, British Colombia. In: Dowdeswell, J.A., Canals, M., Jakobsson, M., Todd, B.J., Dowdeswell, E.K., Hogan, E.K. (Eds.), Atlas of Submarine Glacial Landforms: Modern, Quaternary and Ancient. Geological Society, London, Memoirs, vol. 46. pp. 93–94.
Stacey, C.D., Hill, P.R., Talling, P.J., Enkin, R.J., Hughes Clarke, J.H., Lintern, D.G., 2018. How turbidity current frequency and character varies down a fjord-delta system: combining direct monitoring, deposits and seismic data. Sedimentology. https://doi.org/10.1111/sed.12488. (accepted article).
Syvitski, J.P.M., 1989. On the deposition of sediment within glacier-influenced fjords: oceanographic controls. Mar. Geol. 85, 301–329.
Syvitski, J.P.M., 1991. The changing microfabric of suspended particulate matter – the fluvial to marine transition: flocculation, agglomeration, and palletization. In: Bennet, R.H., Bryant, W.R., Hulbert, M.H. (Eds.), Microstructure of Fine-Grained Sediments. Springer-Verlag, New York, pp. 131–137.
Syvitski, J.P.M., Shaw, J., 1995. Sedimentology and geomorphology of fjords. In: Perillo, G.M.E. (Ed.), Geomorphology and Sedimentology of Estuaries. Elsevier, Amsterdam, pp. 113–178.
Syvitski, J.P.M., Burrell, D.C., Skei, J.M., 1987. Fjords: Processes and Products. Springer, Berlin.
Tanaka, K., 1980. Geographic Contribution to a Periglacial Study of the Hielo Patagónico Norte With Special Reference to the Glacial Outburst Originated From Glacier-Dammed Lago Arco, Chilean Patagonia. Center Company, Tokyo, pp. 97.
Van Daele, M., Bertrand, S., Meyer, I., Moernaut, J., Vandoorne, W., Siani, G., Tanghe, N., Ghazoui, Z., Pino, M., Urrutia, R., De Batist, M., 2016. Late Quaternary evolution of Lago Castor (Chile, 45.6 °S): timing of the deglaciation in northern Patagonia and evolution of the southern westerlies during the last 17 kyr. Quat. Sci. Rev. 133, 130–146. https://doi.org/10.1016/j.quascirev.2015.12.021.
Vendettuoli, D., Clare, M.A., Hughes Clarke, J.E., Vellinga, A., Hizzet, J., Hage, S., Cartigny, M.J.B., Talling, P.J., Waltham, D., Hubbard, S.M., Stacey, C., Lintern, D.G., 2019. Daily bathymetric surveys document how stratigraphy is built and its extreme incompleteness in submarine channels. Earth Planet. Sci. Lett. 515, 231–247.
Verardo, D.J., Froelich, P.N., McIntyre, A., 1990. Determination of organic carbon and nitrogen in marine sediments using the Carlo Erba NA-1500 Analyzer. Deep-Sea Res. 37 (1), 157–1990.
Wils, K., Van Daele, M., Lastras, G., Kissel, C., Lamy, F., Siani, G., 2018. Holocene event record of Aysén fjord (Chilean Patagonia): an interplay of volcanic eruptions, crustal and megathrust earthquakes. J. Geophys. Res. Solid Earth 123 (1), 324–343. https://doi.org/10.1002/2017JB014573.
Wilson, R., Glasser, N.F., Reynolds, J.M., Harrison, S., Anacona, P.I., Schaefer, M., Shannon, S., 2018. Glacial lakes of the Central and Patagonian Andes. Glob. Planet. Chang. 162, 275–291.
Winchester, V., Harrison, S., 2000. Dendrochronology and lichenometry: colonization, growth rates and dating of geomorphogical events on the east side of the North Patagonian Icefield, Chile. Geomorphology 34, 181–194.
Wynn, R.B., Stow, D.A.V., 2002. Classification and characterisation of deep-water sediment waves. Mar. Geol. 192, 7–22.
Wynn, R.B., Piper, D.J.W., Gee, M.J.R., 2002. Generation and migration of coarse-grained sediment waves in turbidity current channels and channel-lobe transition zones. Mar. Geol. 192, 59–78.